Chiral-Induced Spin Selectivity and Non-equilibrium Spin Accumulation in Molecules and Interfaces: A First-Principles Study

Sumit Naskar,[*,†,¶] Vladimiro Mujica,[‡,§] and Carmen Herrmann[*,†,¶]

†*Department of Chemistry, University of Hamburg,* Harbor *Bldg. 610 Luruper Chaussee 149, 22761 Hamburg, Germany*

‡*School of Molecular Sciences, Arizona State University, Arizona, U.S.A.*

¶*The Hamburg Centre for Ultrafast Imaging, University of Hamburg, Luruper Chaussee 149, 22761 Hamburg, Germany*

§*Kimika Fakultatea, Euskal Herriko Unibertsitatea UPV/EHU, and Donostia International Physics Center, Manuel de Lardizabal Pasealekua 3, 20018 Donostia, Euskadi, Spain*

E-mail: sumit.naskar@chemie.uni-hamburg.de; carmen.herrmann@chemie.uni-hamburg.de

Phone: +49 (0)40 42838-2358; +49 (0)40 42838-6934

Abstract

Electrons moving through chiral molecules are selected according to their spin orientation and the helicity of the molecule, an effect known as chiral induced spin selectivity (CISS). The underlying physical mechanism is not yet completely understood. To help elucidate this mechanism, a non-equilibrium Green's function method, combined with a Landauer approach and density functional theory, is applied to carbon helices contacted by gold electrodes, resulting in spin polarization of transmitted electrons. Interestingly, spin polarization is also observed in the non-equilibrium electronic

structure of the junctions. While this spin polarization is small, its sign changes with the direction of current and with the handedness of the molecule. While these calculations were performed with a pure exchange–correlation functional, previous studies suggest that computationally more expensive hybrid functionals may lead to considerably larger spin polarization in the electronic structure. Thus, nonequilibrium spin polarization could be a key component in understanding the CISS mechanism.

Most molecules have closed electronic shells, with all electrons being spin-paired and a net spin of zero. More than two decades ago, a phenomenon surfaced where the electron transport in chiral representatives of such closed-shell molecules was shown to depend on the spin, with the preferred orientation of this spin changing with the handedness of the chiral molecule. This effect is known as chiral induced spin selectivity (CISS)[1–9]. It has been observed in electron transport, electron transfer, electron polarization, and in electron photoemission, involving biomolecules, organic molecules and also inorganic solids, with efficiencies of up to 80-90%.[10–16] It has implications for spintronics, enantioselective reactions, long-range charge transport in biological molecules, chiral recognition in intermolecular interactions,[17,18] and quantum information science.[4,5,10,19–23] The mechanism behind CISS is not understood at present, although it is clear that it is related to the interplay of space- and time-reversal-symmetry breaking and spin–orbit coupling (SOC).[24–28] Several competing (or possibly complementary) suggestions about the "missing" underlying physics have been made, ranging from electron–phonon interactions to electron correlations to non-equilibrium, current-induced spin accumulation on the molecule–electrode interface or on the molecule. In this letter, we explore the importance of the latter part of the mechanism, nonequilibrium spin accumulation for CISS.

Nonequilibrium spin accumulation has also been discussed in other contexts, for example in spin Hall devices[29] and as an essential ingredient for understanding topological insulators.[30] One way of thinking about such spin accumulation in CISS[5,24] is based on the consideration

that chiral molecules only give passage for electrons with specific spin, such that the other component of the spin may accumulate at the interface or on the molecule. This may allow designing a spin-splitter where spin up/down ($\uparrow/\downarrow$) accumulates in different spatial regions.[31] Nonequilibrium spin accumulation in CISS has been suggested based on several experimental observations. One are spin Hall measurements, where the preference for electrons of a certain spin orientation to be transported through chiral layers is thought to result in this spin orientation becoming dominant at the interface between the chiral layer and an electrode, leading to a magnetic field which Hall devices can measure.[32–34] Another important experimental observation is the preference of magnetic metal surfaces to adsorb chiral molecules of a certain handedness.[10,11,17,35,36] This is only observable in the adsorption kinetics but not in the thermodynamics.[37] It has been attributed to the charge transfer upon adsorption being accompanied by spin polarization of the electronic structure due to CISS, and since the charge transfer is a transient phenomenon, so is the spin polarization. The orientation of the transient spin at the adsorbing end of the molecule depends on the molecule's handedness, and accordingly, exchange interactions between this spin and the surface spins will depend on the handedness, affecting the adsorption kinetics. This can be exploited for enantiomer separation.[38] A similar mechanism leads to enantioselectivity in electrochemical reactions on magnetized electrodes[11,39] and in Diels–Alder reactions catalyzed by magnetic nanoparticles.[21] In a related experiment, Ghosh *et al.* performed Kelvin-probe force microscopy on chiral self-assembled monolayers coating ferromagnetic thin-film electrodes, revealing that how much the electrons of the ferromagnet penetrate into the chiral layer depends on the ferromagnet's magnetization direction and on the chiral layer's helicity.[36]

From the theoretical side, nonequilibrium spin accumulation has been discussed based on different model Hamiltonians and mechanisms.[18,40] The main challenge to reproduce experimental results with theoretical approaches based on tight-binding or scattering lies in the need for including unrealistically high values of spin–orbit coupling.[25–28] To achieve similar magnitudes of spin polarization as in the experiments, there are several reports which sug-

gest this large value of SOC as originating from the metal surface to which the molecules are attached. Alwan *et al.* proposed that the CISS effect is generated as a consequence of the solenoidal field inside the chiral molecule and large SOC in the electrode, which provides spin transfer-torque between the surface of the electrode and the molecule.[41] Similarly Gersten *et al.*[42] and Liu *et al.*[43] suggested that the interface plays a major role. In the same line Dalum *et al.* argued that the spin–orbit coupling combined with the chiral molecule and magnetized lead in one side of the junction will magnetize the non-magnetic lead on the other side.[44] Another suggestion for rationalizing the large magnitude of CISS is an interplay between SOC and electron–phonon coupling.[40,45–49] Very recently, Das *et al.* suggested in a combined experimental and theoretical study that CISS increases with temperature due to electron–phonon coupling. They also suggested that a mechanism combining spin–orbit and electron–phonon coupling in CISS may lead to nonequilibrium spin accumulation on the molecule.[40]

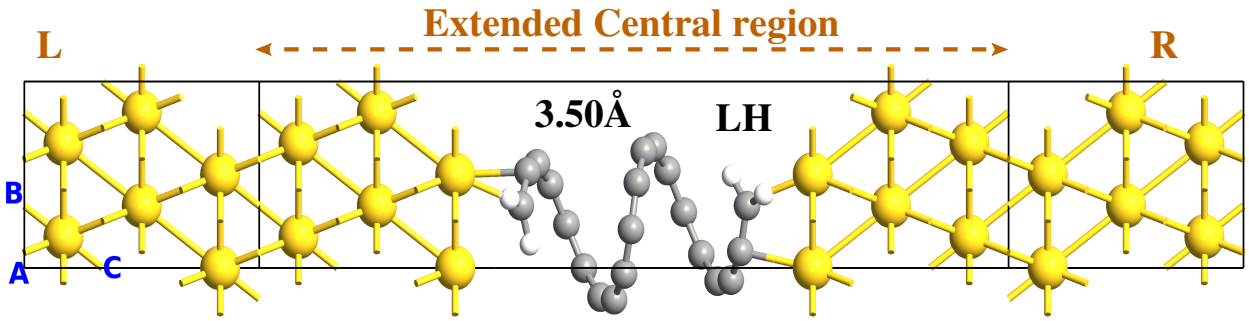

Figure 1: Atomistic model for a single molecule junction with $3 \times 2 \times 2$ Au(111) electrodes, where the extended central region contains the chiral molecule and some layers of gold. Yellow balls indicate gold atoms, grey ones carbon atoms, and white ones hydrogen atoms. The transport direction is the C direction, A and B are perpendicular to the transport direction. L is the left-electrode which acts as source and R is the right electrode which acts as a drain.

Atomistic first-principles simulations can go one step beyond models based on more simple Hamiltonians, in particular they can deliver a realistic description of how electron densities get (spin-)polarized by electric fields, current or other stimuli. So far, first-principles simulations of nonequilibrium spin polarization in the electronic structure as caused by CISS

have not been reported. To evaluate such nonequilibrium spin polarization from first principles, we consider an equidistant model carbon helix with hydrogen saturation at both ends. The helix was attached between two metallic Au(111) electrodes (see Fig 1), and the calculations include an external bias to evaluate electric current employing non–equilibrium density matrices in the self-consistent-field algorithm under periodic boundary conditions. This translates into a self-consistent determination of the voltage profile in the junction and orbital occupancy, an effect that is often neglected in simple transmission calculations (see Supporting Information for further details on structural and computational settings).

An equidistant carbon helix is a rough model of an actual molecule. It will have a smaller gap between occupied and unoccupied effective single-particle levels than most realistic systems, and it is chemically and structurally not stable. We study it here, as in several previous studies,[6,7,50,51] because it shows relatively large CISS-induced polarizations, which allow for a clear distinction between signal and noise when analyzing our data.

As in several previous theoretical descriptions of CISS, we consider coherent transport of electrons (Landauer regime).[6–8,41,43,50,52,53] While this cannot take into account potentially important dephasing and dissipation processes,[25,26] it has proven highly valuable for describing charge and spin transport through molecular and nanoscale junctions up to lengths of a few nanometers,[54–56] and we expect it to give a good description of an important part of the mechanism underlying CISS. As CISS is a non-equilibrium phenomenon, we consider the applied bias voltage and calculate density matrices based on non-equilibrium Green's functions and density functional theory (NEGF-DFT), employing a two-component framework including spin–orbit coupling, as implemented in the Atomistix Toolkit (ATK) program package.[57] Since the availability of different exchange–correlation functionals in combination with such an approach is currently limited, we employ the local density approximation (LDA; see Supporting Information for computational details). Due to the helical molecule being built from carbon atoms, spin–orbit coupling in the molecule is small and most of the SOC

on the molecule is coming from the electrode–molecule interface.[58,59]

Within a Landauer coherent tunneling picture, the polarization for transmitted electron reads, in percent,

$$P = \frac{T_{RL}^{\uparrow\uparrow} + T_{RL}^{\downarrow\uparrow} - T_{RL}^{\uparrow\downarrow} - T_{RL}^{\downarrow\downarrow}}{2T_{RL}} \times 100, \tag{1}$$

where L/R represents the left/right electrode of the device and $2T_{RL} = T_{RL}^{\uparrow\uparrow}+T_{RL}^{\downarrow\uparrow}+T_{RL}^{\uparrow\downarrow}+T_{RL}^{\downarrow\downarrow}$ is twice the total transmission [1]. The spin-dependent transmission functions are given by:

$$T_{RL}^{\uparrow\uparrow} = \mathrm{Tr}[\Gamma_L^{\uparrow\uparrow} G^{\uparrow\uparrow} \Gamma_R^{\uparrow\uparrow} (G^{\uparrow\uparrow})^\dagger] \tag{2}$$

$$T_{RL}^{\downarrow\uparrow} = \mathrm{Tr}[\Gamma_L^{\downarrow\uparrow} G^{\downarrow\uparrow} \Gamma_R^{\downarrow\uparrow} (G^{\downarrow\uparrow})^\dagger] \tag{3}$$

$$T_{RL}^{\uparrow\downarrow} = \mathrm{Tr}[\Gamma_L^{\uparrow\downarrow} G^{\uparrow\downarrow} \Gamma_R^{\uparrow\downarrow} (G^{\uparrow\downarrow})^\dagger] \tag{4}$$

$$T_{RL}^{\downarrow\downarrow} = \mathrm{Tr}[\Gamma_L^{\downarrow\downarrow} G^{\downarrow\downarrow} \Gamma_R^{\downarrow\downarrow} (G^{\downarrow\downarrow})^\dagger]. \tag{5}$$

$T_{RL}^{\downarrow\uparrow}$ and $T_{RL}^{\uparrow\downarrow}$ are the spin-flip components which are usually smaller than the spin-conserving components $T_{RL}^{\uparrow\uparrow}$ and $T_{RL}^{\downarrow\downarrow}$, similar to the study of Maslyuk *et al.*[7] In Atk, the spin-flip terms in the transmission are dropped, such that the spin-polarization reads

$$P' = \frac{T_{RL}^{\uparrow\uparrow} - T_{RL}^{\downarrow\downarrow}}{2T'_{RL}} \times 100, \tag{6}$$

and the total transmission function reads

$$2T'_{RL} = T_{RL}^{\uparrow\uparrow} + T_{RL}^{\downarrow\downarrow}. \tag{7}$$

$\Gamma_{L/R}^{\sigma\sigma'}$ in Equations (2) to (5) are the bulk broadening functions for the left or right electrode (see Fig 1) written as

$$\Gamma_{L/R}^{\sigma\sigma'} = \frac{1}{i}[\Sigma_{L/R}^{\sigma\sigma'} - (\Sigma_{L/R}^{\sigma\sigma'})^\dagger] \tag{8}$$

[1] The factor of 2 stems from the fact that usually, transmission is defined for a single electron of specific spin orientation.

where $\sigma\sigma'$ are spin indices ($\uparrow$ / $\downarrow$). The Green's function can be written as

$$G^{\sigma\sigma'}(\epsilon) = [(\epsilon + i\delta_+)S^{\sigma\sigma'} - H^{\sigma\sigma'} - \Sigma_L^{\sigma\sigma'}(\epsilon) - \Sigma_R^{\sigma\sigma'}(\epsilon)]^{-1}, \tag{9}$$

where δ_+ is an infinitesimally small positive number, coming due to boundary conditions,[57,60] S and H are overlap and the effective single-particle Hamiltonian matrix, respectively, expressed in the basis of atom-centered basis functions. $\Sigma_{L/R}$ is the electronic self-energy for the left/right electrode. In non-equilibrium, the Fermi energy will shift from its equilibrium value, and the complex contour integration for evaluating the density matrix (see below) will be calculated for the shifted contour due to two or more chemical potentials.

As in standard DFT, the electronic structure (the Kohn–Sham determinant constructed from effective single-particle functions) is evaluated iteratively based on a self-consistent-field algorithm. In contrast to standard DFT, the density matrix is evaluated from non-equilibrium Green's functions, to take into account the effect of bias voltage and open-boundary conditions. This non-equilibrium density matrix can be written as[57,61]

$$\tilde{D}^{(\sigma\sigma')} = D_{L/R}^{eq(\sigma\sigma')} + \Delta_{R/L}^{neq(\sigma\sigma')} \tag{10}$$

where

$$D_{L/R}^{eq(\sigma\sigma')} = -\frac{1}{2\pi}\mathrm{Im}\int_{-\infty}^{\infty} d\epsilon\ G^{\sigma\sigma'}(\epsilon + i\delta_+)n_F(\epsilon - \mu_{L/R}). \tag{11}$$

is the equilibrium part, and

$$\Delta_{R/L}^{neq(\sigma\sigma')} = \int_{-\infty}^{\infty} d\epsilon\ \rho_{R/L}^{\sigma\sigma'}(\epsilon)[n_F(\epsilon - \mu_{R/L}) - n_F(\epsilon - \mu_{L/R})] \tag{12}$$

is the non-equilibrium part. $n_F(\epsilon - \mu_{L/R}) = f\left(\frac{\epsilon - \mu_{L/R}}{\kappa_B T_{L/R}}\right)$ denotes the Fermi distribution function and $\mu_{L/R}$ the chemical potential for the left/right electrode. The spectral density

function $\rho_{L/R}$ can be written as

$$\rho^{\sigma\sigma'}_{L/R}(\epsilon) = \frac{1}{2\pi} G^{\sigma\sigma'}(\epsilon)\Gamma^{\sigma\sigma'}_{L/R}G^{\sigma\sigma'\dagger}(\epsilon). \tag{13}$$

(details can be found in Refs.[61,62]).

When evaluating the spin polarization in the transmission and in the nonequilibrium electronic structure, we take one of the gold electrodes to mimic a perfect spin filter by just considering the transmission of one spin orientation or the other. Importantly, having no magnetic electrode in the system ensures that any nonequilibrium spin density in the electronic structure is only due to CISS as emerging from a closed-shell chiral atomistic structure. For comparison, data with a magnetic Nickel electrode are provided in the Supporting Information (Figures S19, S20, and S21). It is also clear that one cannot measure the CISS effect in experiment at zero bias — here, zero bias refers to the bias voltage at which the electronic structure underlying the transmission function is evaluated, which is a good approximation for the electronic structure at low bias.[6]

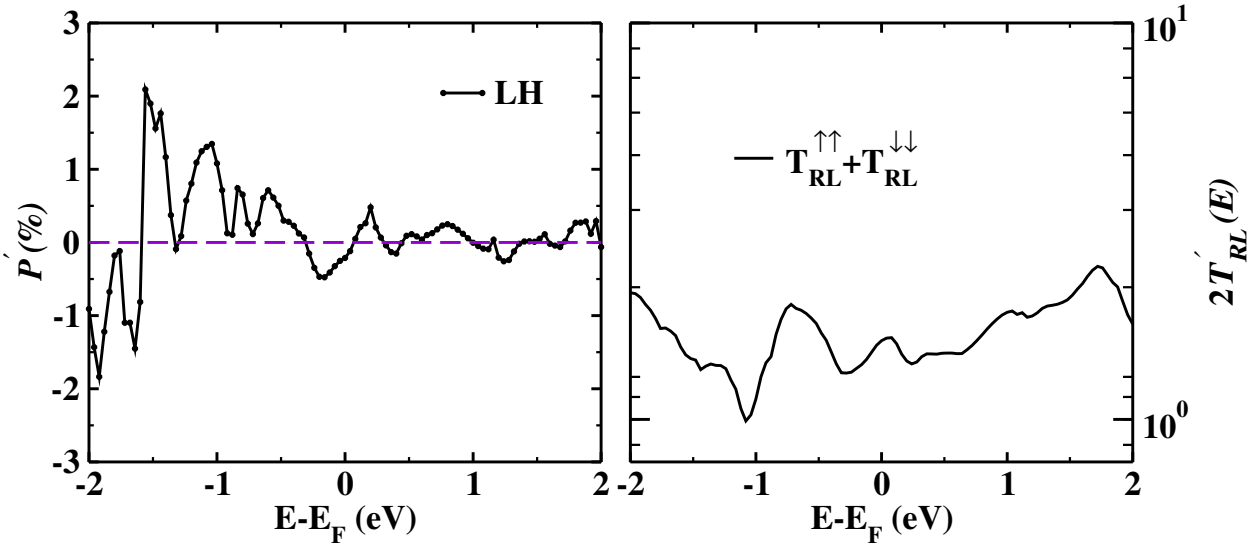

Figure 2: Spin polarization of the transmitted electrons and sum of the spin-conserving transmission contributions for a junction with $3 \times 2 \times 2$ Au(111) electrodes. The data are shown for zero bias, i.e., the electronic structure is the equilibrium one.

In Figure 2, the polarization of the transmitted electrons, P, and the sum of the spin-conserving parts of the transmission, calculated from the zero-bias electronic structure, are plotted for a left-handed helix. Similar to previous studies, the polarization is on the order of below one percent close to the Fermi energy, and a few percent when covering a broader range of energies. The value at the Fermi energy is very small. Employing a hybrid functional may lead to a much larger (and potentially more realistic) polarization[50] (also compare Figure S3 in the Supporting Information). However, implementations combining hybrid functionals with nonequilibrium density matrices and two-component DFT under inclusion of SOC are not broadly accessible in existing electronic structure codes. This only affect the quantitative and not the qualitative conclusions from our study, as trends are expected to be consistent over different types of functionals. The overall transmission (which is summed up here for both spin components) is close to values between 1 and 2 for a broad range of energies. This is consistent with the electronic structure of an equidistant carbon chain, which would be metallic at infinite length. This close-to-metallic character is also reflected in the nearly linear current–voltage curves (Figure S9 in the Supporting Information).

When reversing the chirality, the polarization reverses sign (Figure S6), and the total transmission remains similar (Figure S7) [2]. There are more fluctuations in the polarization curve than in the one previously found with a cluster-based approach.[6,8,50] This is in line with the strongly oscillating P found for a carbon helix in Ref.[7] employing periodic boundary conditions and a pure exchange–correlation functional.

Besides the differences between exchange–correlation functionals and cluster-based versus periodic-boundary approaches (compare Figures S4 and S5 in the Supporting Information), another possible reason for this difference to previous data could be electronic interactions with the next-nearest unit cell: If we repeat the unit cell perpendicular to the transport direction for our junction with $3 \times 2 \times 2$ Au(111) electrodes, the shortest C−C distance

[2]Small differences may be due to numerical errors (the up and down components of transmission at zero bias can be found in Figure S8).

is 2.96 Å, which is inside the sum of the van-der-Waals radii (3.50 Å). This interaction can be reduced substantially by using larger $3 \times 3 \times 2$ electrodes, which will increase the unit cell volume (see Figure S6, top, in the SI). However, this also drastically increases the computational effort. Also, as can be seen from Figure 3, while going to larger unit cells and thus reducing interactions makes the transmission look somewhat less "metallic" (with more discernible peaks and lower values between them), the polarization does not change substantially compared to the smaller unit cell.

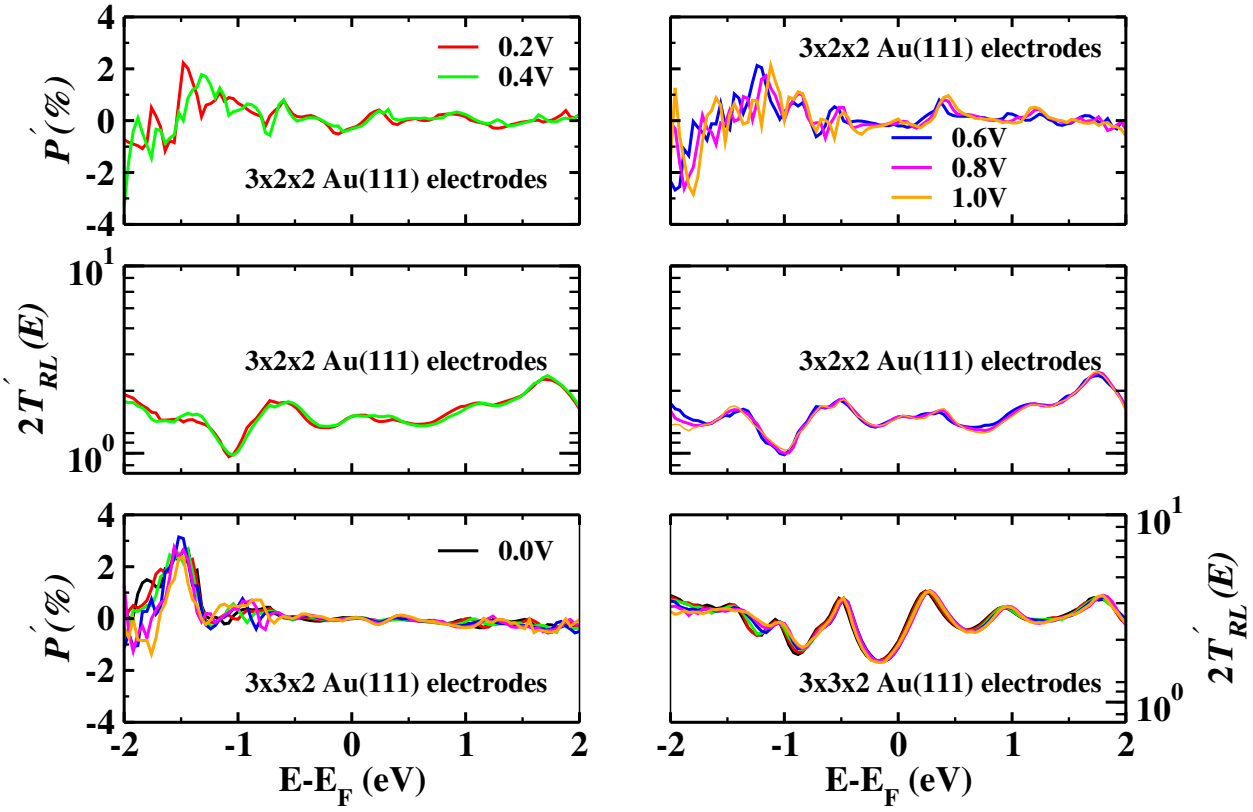

Figure 3: Spin polarization and transmission functions for $3 \times 2 \times 2$ Au(111) (top and middle panels) and $3 \times 3 \times 2$ Au(111) electrodes (bottom panel). The electronic structure is evaluated for situations out of equilibrium, corresponding to the bias voltages indicated in the plots.

Within the Landauer picture, a difference in transport properties for electrons of different spins (as reflected in spin-dependent transmission functions) implies that in nonequilibrium, electrons of different spins will "see" the Green's function differently. They can, therefore, assume different density matrices, giving rise to non-equilibrium spin polarization in the

electronic structure, or, in other words, to nonzero spin density resulting from current flow through chiral systems in the presence of spin–orbit coupling. We will also refer to this process as "spin accumulation" in this work. Even though this term evokes a mental picture of individual, integer electrons transferring through a junction and getting "stuck" somewhere along the way (e.g., at the interface), spin accumulation by the mechanism described above can lead to a continuum of noninteger values for the amount of unpaired spin forming on the junction in nonequilibrium.

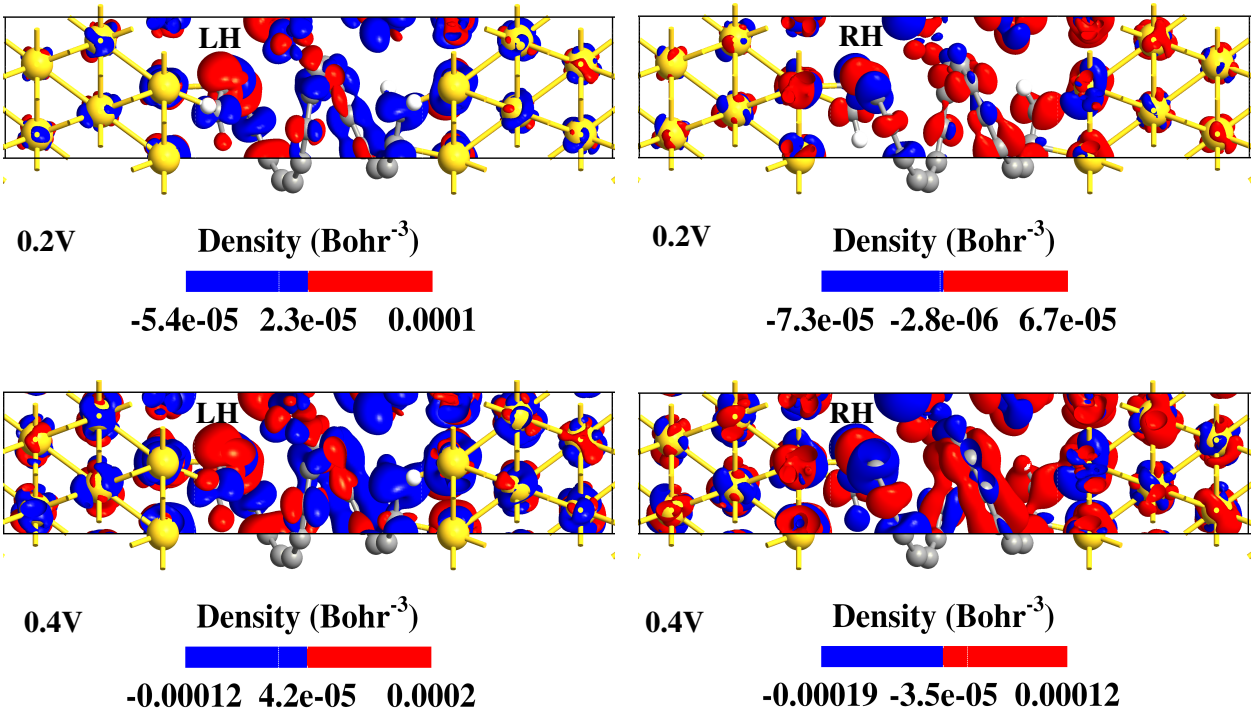

Figure 4: Non-equilibrium spin polarization of the electronic structure: spin density isosorfaces for left-handed (left) and right-handed (right) helices, for two different bias voltages for junctions with $3 \times 2 \times 2$ Au(111) electrodes. The isosurface value was $5 \cdot 10^{-6}$ Bohr^{-3}. The values at the edges of the color bar show the maximum values (positive/negative) assumed by the spin densities.

We would expect nonequilibrium spin polarization to change sign if we change the handedness of the chiral molecule or reverse the direction of the current. In Figure 4, non-equilibrium spin-polarization in the electronic structure (resulting in nonzero spin density) is plotted as a function of forward biases for helices of different handedness, with the small unit cell ($3 \times 2 \times 2$ Au(111) electrodes). It leads to regions of positive and negative spin densities,

which roughly balance each other. While the nonequilibrium spin density is small and should therefore be interpreted with some caution, its qualitative behaviour is physically reasonable: The spin density changes sign for different handedness (Figure 4, Figure S11) as well as for different directions of electric current (Figure S10). As the voltage goes up, so does the nonequilibrium spin density (Figure 4 in the main text and Figure S12 in the Supporting Information).

As can be seen in Figure 3, the transmission and the polarization of transmitted electrons (P) are not strongly affected by the bias voltage. At first sight, this would indicate that the nonequilibrium spin density in the electronic structure does not play an important role in electron transport and its spin polarization. It should be kept in mind though that this nonequilibrium spin density has small values here, and that these small values may be an artifact of the pure approximate exchange–correlation functional employed in our calculations for technical reasons. As discussed above, including exact exchange in the functional strongly increases P.[50] It also leads to more pronounced spin polarization in the electronic structure.[63,64] Thus, it does not seem unlikely that including exact exchange could also increase the nonequilibrium spin density in the electronic structure, and thus lead to stronger effects of bias voltage on P.

The CISS-induced nonequilibrium spin polarization in the electronic structure may be related to an enhanced polarizability resulting from the interactions with helices in adjacent unit cells. Indeed, as shown in Figure S11 in the Supporting Information, the nonequilibrium spin density is somewhat smaller when looking at the system with the larger unit cell ($3 \times 3 \times 2$ electrodes).

The spin is accumulating mostly on the helices and right at the interface, and to a lesser degree on the gold electrodes. Again, this should be interpreted with some caution, as the proper description of molecule–metal interfaces is a challenge for present-day approximate DFT. What is interesting and possibly transferable, however, is that the nonequilibrium spin

density is largest in the areas where the potential drops the most (compare Figure 5).

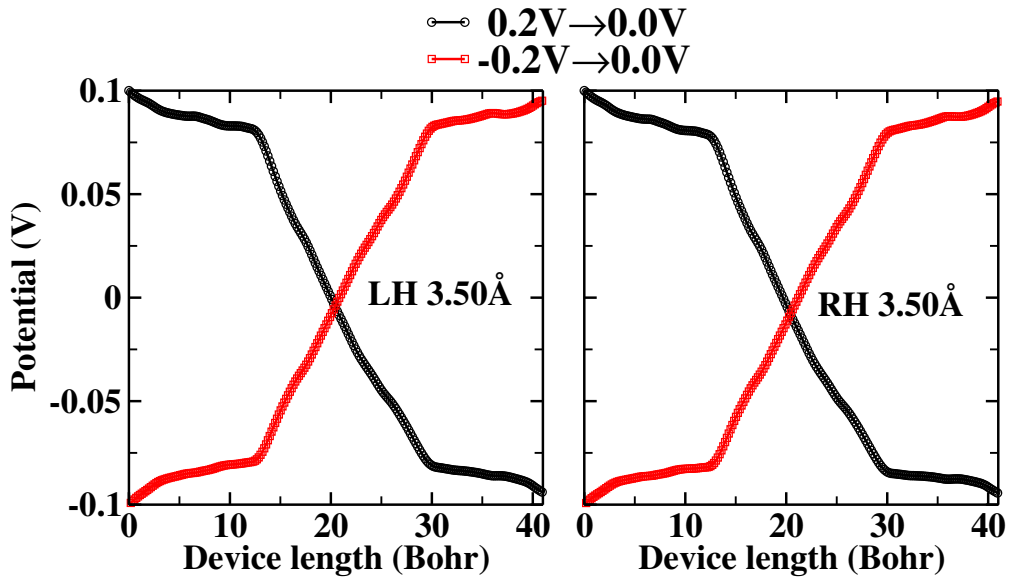

Figure 5: Potential drop for junctions with $3 \times 2 \times 2$ Au(111) electrodes for low biases (0.2V and -0.2V). The potential is evaluated solving Poisson's equation, see Section S2 in the SI.

To conclude, when modeling electron transport through a carbon-chain helix with first-principles methods, combining two-component DFT, SOC, and Green's function techniques which take into account the effect of nonequilibrium conditions on the electronic structure, a small but physically consistent nonequilibrium spin density is induced by the current on the molecule, and to a lesser degree on the electrodes. The small magnitude may result from employing a pure exchange-–correlation functional, as previous studies suggest that computationally more expensive hybrid functionals lead to larger spin polarizations in electronic structures. The nonequilibrium spin density changes sign when reversing the helicity of the chiral molecule or the current direction, and it increases with bias voltage (and, accordingly, with current). Also, this spin density is larger for smaller unit cells, which lead to stronger interactions between adjacent helices. This is in line with DFT calculations suggesting that the electronic structures of monolayers of helical peptides are easier to spin-polarize than individual peptides.[17] As CISS experiments are usually carried out for such monolayers (or for individual molecules in a solvent environment that may equally help with spin polariz-

ability[65]), our results suggest that nonequilibrium spin polarization may play an important role in CISS and in understanding its underlying mechanism.

Acknowledgement

We would like to thank the high-performance computing centre at the University of Hamburg for computational resources. This work is supported by the Cluster of Excellence "CUI: Advanced Imaging of Matter" of the Deutsche Forschungsgemeinschaft (DFG) — EXC 2056 — project ID 390715994. V.M. acknowledges a Fellowship from Ikerbasque, the Basque Foundation for Science.

Supporting Information Available

Computational details, optimization and comparison of computational parameters and exchange–correlation functionals; total and spin-resolved transmission functions; $I - V$ curves; spin densities for larger bias voltages, different current directions and helicities, and larger electrodes; potential drop at larger bias voltages and for larger electrodes; noncollinear Mulliken spin populations; spin polarization for junctions with one Ni electrode; input files and atomic coordinates for all calculations can be found in the Supporting information (SI).

References

(1) Ray, K.; Ananthavel, S.; Waldeck, D.; Naaman, R. Asymmetric scattering of polarized electrons by organized organic films of chiral molecules. *Science* **1999**, *283*, 814–816.

(2) Naaman, R.; Paltiel, Y.; Waldeck, D. H. Chiral induced spin selectivity gives a new twist on spin-control in chemistry. *Accounts of Chemical Research* **2020**, *53*, 2659–2667.

(3) Naaman, R.; Paltiel, Y.; Waldeck, D. H. Chiral molecules and the electron spin. *Nature Reviews Chemistry* **2019**, *3*, 250–260.

(4) Naaman, R.; Waldeck, D. H. Spintronics and chirality: Spin selectivity in electron transport through chiral molecules. *Annual review of physical chemistry* **2015**, *66*, 263–281.

(5) Aiello, C. D.; Abendroth, J. M.; Abbas, M.; Afanasev, A.; Agarwal, S.; Banerjee, A. S.; Beratan, D. N.; Belling, J. N.; Berche, B.; Botana, A., et al. A Chirality-Based Quantum Leap. *ACS nano* **2022**, *16*, 4989–5035.

(6) Zöllner, M. S.; Varela, S.; Medina, E.; Mujica, V.; Herrmann, C. Insight into the origin of chiral-induced spin selectivity from a symmetry analysis of electronic transmission. *Journal of Chemical Theory and Computation* **2020**, *16*, 2914–2929.

(7) Maslyuk, V. V.; Gutierrez, R.; Dianat, A.; Mujica, V.; Cuniberti, G. Enhanced magnetoresistance in chiral molecular junctions. *The journal of physical chemistry letters* **2018**, *9*, 5453–5459.

(8) Naskar, S.; Saghatchi, A.; Mujica, V.; Herrmann, C. Common Trends of Chiral Induced Spin Selectivity and Optical Dichroism with Varying Helix Pitch: A First-Principles Study. *Israel Journal of Chemistry* **2022**, e202200053.

(9) Matsuura, Y. Coherent spin transport in a natural metalloprotein molecule. *Journal of Applied Physics* **2021**, *130*, 184301.

(10) Naaman, R.; Paltiel, Y.; Waldeck, D. H. Chiral molecules and the spin selectivity effect. *The Journal of Physical Chemistry Letters* **2020**, *11*, 3660–3666.

(11) Bloom, B.; Lu, Y.; Metzger, T.; Yochelis, S.; Paltiel, Y.; Fontanesi, C.; Mishra, S.; Tassinari, F.; Naaman, R.; Waldeck, D. Asymmetric reactions induced by electron spin polarization. *Physical Chemistry Chemical Physics* **2020**, *22*, 21570–21582.

(12) Lu, H.; Xiao, C.; Song, R.; Li, T.; Maughan, A. E.; Levin, A.; Brunecky, R.; Berry, J. J.; Mitzi, D. B.; Blum, V., et al. Highly distorted chiral two-dimensional tin iodide perovskites for spin polarized charge transport. *Journal of the American Chemical Society* **2020**, *142*, 13030–13040.

(13) Kim, Y.-H.; Zhai, Y.; Lu, H.; Pan, X.; Xiao, C.; Gaulding, E. A.; Harvey, S. P.; Berry, J. J.; Vardeny, Z. V.; Luther, J. M., et al. Chiral-induced spin selectivity enables a room-temperature spin light-emitting diode. *Science* **2021**, *371*, 1129–1133.

(14) Kulkarni, C.; Mondal, A. K.; Das, T. K.; Grinbom, G.; Tassinari, F.; Mabesoone, M. F.; Meijer, E.; Naaman, R. Highly Efficient and Tunable Filtering of Electrons' Spin by Supramolecular Chirality of Nanofiber-Based Materials. *Advanced Materials* **2020**, *32*, 1904965.

(15) Lu, H.; Wang, J.; Xiao, C.; Pan, X.; Chen, X.; Brunecky, R.; Berry, J. J.; Zhu, K.; Beard, M. C.; Vardeny, Z. V. Spin-dependent charge transport through 2D chiral hybrid lead-iodide perovskites. *Science advances* **2019**, *5*, eaay0571.

(16) Qian, Q.; Ren, H.; Zhou, J.; Wan, Z.; Zhou, J.; Yan, X.; Cai, J.; Wang, P.; Li, B.; Sofer, Z., et al. Chiral molecular intercalation superlattices. *Nature* **2022**, *606*, 902–908.

(17) Dianat, A.; Gutierrez, R.; Alpern, H.; Mujica, V.; Ziv, A.; Yochelis, S.; Millo, O.; Paltiel, Y.; Cuniberti, G. Role of exchange interactions in the magnetic response and intermolecular recognition of chiral molecules. *Nano Letters* **2020**, *20*, 7077–7086.

(18) Geyer, M.; Gutierrez, R.; Mujica, V.; Silva, J.; Dianat, A.; Cuniberti, G. The contribution of the Chirality-Induced Spin Selectivity (CISS) effect to the dispersion interaction between chiral molecules. *arXiv preprint arXiv:2106.06350* **2021**,

(19) Shang, Z.; Liu, T.; Yang, Q.; Cui, S.; Xu, K.; Zhang, Y.; Deng, J.; Zhai, T.; Wang, X. Chiral-Molecule-Based Spintronic Devices. *Small* **2022**, *18*, 2203015.

(20) Wang, C.; Guo, A.-M.; Sun, Q.-F.; Yan, Y. Efficient Spin-Dependent Charge Transmission and Improved Enantioselective Discrimination Capability in Self-Assembled Chiral Coordinated Monolayers. *The Journal of Physical Chemistry Letters* **2021**, *12*, 10262–10269.

(21) Metzger, T. S.; Siam, R.; Kolodny, Y.; Goren, N.; Sukenik, N.; Yochelis, S.; Abu-Reziq, R.; Avnir, D.; Paltiel, Y. Dynamic Spin-Controlled Enantioselective Catalytic Chiral Reactions. *The Journal of Physical Chemistry Letters* **2021**, *12*, 5469–5472.

(22) Mishra, S.; Pirbadian, S.; Mondal, A. K.; El-Naggar, M. Y.; Naaman, R. Spin-dependent electron transport through bacterial cell surface multiheme electron conduits. *Journal of the American Chemical Society* **2019**, *141*, 19198–19202.

(23) Banerjee-Ghosh, K.; Ghosh, S.; Mazal, H.; Riven, I.; Haran, G.; Naaman, R. Long-range charge reorganization as an allosteric control signal in proteins. *Journal of the American Chemical Society* **2020**, *142*, 20456–20462.

(24) Evers, F.; Aharony, A.; Bar-Gill, N.; Entin-Wohlman, O.; Hedegård, P.; Hod, O.; Jelinek, P.; Kamieniarz, G.; Lemeshko, M.; Michaeli, K., et al. Theory of Chirality Induced Spin Selectivity: Progress and Challenges. *Advanced Materials* **2021**, 2106629.

(25) Guo, A.-M.; Sun, Q.-f. Spin-selective transport of electrons in DNA double helix. *Physical review letters* **2012**, *108*, 218102.

(26) Guo, A.-M.; Sun, Q.-F. Spin-dependent electron transport in protein-like single-helical molecules. *Proceedings of the National Academy of Sciences* **2014**, *111*, 11658–11662.

(27) Varela, S.; Mujica, V.; Medina, E. Effective spin-orbit couplings in an analytical tight-binding model of DNA: Spin filtering and chiral spin transport. *Physical Review B* **2016**, *93*, 155436.

(28) Salazar, S. V.; Mujica, V.; Medina, E. Spin-orbit coupling modulation in dna by mechanical deformations. *CHIMIA International Journal for Chemistry* **2018**, *72*, 411–417.

(29) Takahashi, S.; Maekawa, S. Spin current, spin accumulation and spin Hall effect. *Science and Technology of Advanced Materials* **2008**, *9*, 014105.

(30) Liu, Y.; Besbas, J.; Wang, Y.; He, P.; Chen, M.; Zhu, D.; Wu, Y.; Lee, J. M.; Wang, L.; Moon, J., et al. Direct visualization of current-induced spin accumulation in topological insulators. *Nature communications* **2018**, *9*, 1–6.

(31) Hu, P.-J.; Wang, S.-X.; Chen, X.-F.; Gao, X.-H.; Fang, T.-F.; Guo, A.-M.; Sun, Q.-F. Charge Transport in a Multiterminal DNA Tetrahedron: Interplay among Contact Position, Disorder, and Base-Pair Mismatch. *Physical Review Applied* **2022**, *17*, 024074.

(32) Bullard, G.; Tassinari, F.; Ko, C.-H.; Mondal, A. K.; Wang, R.; Mishra, S.; Naaman, R.; Therien, M. J. Low-resistance molecular wires propagate spin-polarized currents. *Journal of the American Chemical Society* **2019**, *141*, 14707–14711.

(33) Ko, C.-H.; Zhu, Q.; Tassinari, F.; Bullard, G.; Zhang, P.; Beratan, D. N.; Naaman, R.; Therien, M. J. Twisted molecular wires polarize spin currents at room temperature. *Proceedings of the National Academy of Sciences* **2022**, *119*, e2116180119.

(34) Eckshtain-Levi, M.; Capua, E.; Refaely-Abramson, S.; Sarkar, S.; Gavrilov, Y.; Mathew, S. P.; Paltiel, Y.; Levy, Y.; Kronik, L.; Naaman, R. Cold denaturation induces inversion of dipole and spin transfer in chiral peptide monolayers. *Nature communications* **2016**, *7*, 1–9.

(35) Ziv, A.; Saha, A.; Alpern, H.; Sukenik, N.; Baczewski, L. T.; Yochelis, S.; Reches, M.; Paltiel, Y. AFM-Based Spin-Exchange Microscopy Using Chiral Molecules. *Advanced Materials* **2019**, *31*, 1904206.

(36) Ghosh, S.; Mishra, S.; Avigad, E.; Bloom, B. P.; Baczewski, L.; Yochelis, S.; Paltiel, Y.; Naaman, R.; Waldeck, D. H. Effect of chiral molecules on the electron's spin wavefunction at interfaces. *The journal of physical chemistry letters* **2020**, *11*, 1550–1557.

(37) Lu, Y.; Bloom, B. P.; Qian, S.; Waldeck, D. H. Enantiospecificity of Cysteine Adsorption on a Ferromagnetic Surface: Is It Kinetically or Thermodynamically Controlled? *J. Chem. Phys. Lett.* **2021**, *12*, 7854–7858.

(38) Banerjee-Ghosh, K.; Dor, O. B.; Tassinari, F.; Capua, E.; Yochelis, S.; Capua, A.; Yang, S.-H.; Parkin, S. S.; Sarkar, S.; Kronik, L., et al. Separation of enantiomers by their enantiospecific interaction with achiral magnetic substrates. *Science* **2018**,

(39) Metzger, T. S.; Mishra, S.; Bloom, B. P.; Goren, N.; Neubauer, A.; Shmul, G.; Wei, J.; Yochelis, S.; Tassinari, F.; Fontanesi, C.; Waldeck, D. H.; Paltiel, Y.; Naaman, R. The Electron Spin as a Chiral Reagent. *Angew. Chem. Int. Ed.* **2019**, *59*, 1653–1658.

(40) Das, T. K.; Tassinari, F.; Naaman, R.; Fransson, J. Temperature-Dependent Chiral-Induced Spin Selectivity Effect: Experiments and Theory. *The Journal of Physical Chemistry C* **2022**, *126*, 3257–3264.

(41) Alwan, S.; Dubi, Y. Spinterface Origin for the Chirality-Induced Spin-Selectivity Effect. *Journal of the American Chemical Society* **2021**, *143*, 14235–14241.

(42) Gersten, J.; Kaasbjerg, K.; Nitzan, A. Induced spin filtering in electron transmission through chiral molecular layers adsorbed on metals with strong spin-orbit coupling. *The Journal of chemical physics* **2013**, *139*, 114111.

(43) Liu, Y.; Xiao, J.; Koo, J.; Yan, B. Chirality-driven topological electronic structure of DNA-like materials. *Nature materials* **2021**, *20*, 638–644.

(44) Dalum, S.; Hedegård, P. Theory of chiral induced spin selectivity. *Nano letters* **2019**, *19*, 5253–5259.

(45) Fransson, J. Vibrational origin of exchange splitting and chiral-induced spin selectivity. *Physical Review B* **2020**, *102*, 235416.

(46) Teh, H.-H.; Dou, W.; Subotnik, J. E. Spin Polarization through A Molecular Junction Based on Nuclear Berry Curvature Effects. *arXiv preprint arXiv:2111.12815* **2021**,

(47) Chandran, S. S.; Wu, Y.; Teh, H.-H.; Waldeck, D. H.; Subotnik, J. E. Electron transfer and spin–orbit coupling: Can nuclear motion lead to spin selective rates? *The Journal of Chemical Physics* **2022**, *156*, 174113.

(48) Bian, X.; Wu, Y.; Teh, H.-H.; Zhou, Z.; Chen, H.-T.; Subotnik, J. E. Modeling nonadiabatic dynamics with degenerate electronic states, intersystem crossing, and spin separation: A key goal for chemical physics. *J. Chem. Phys.* **2021**, *154*, 110901.

(49) Wu, Y.; Subotnik, J. E. Electronic spin separation induced by nuclear motion near conical intersections. *Nat Commun* **2021**, *12*, 700.

(50) Zöllner, M. S.; Saghatchi, A.; Mujica, V.; Herrmann, C. Influence of electronic structure modeling and junction structure on first-principles chiral induced spin selectivity. *Journal of Chemical Theory and Computation* **2020**, *16*, 7357–7371.

(51) Dednam, W.; García-Blázquez, M. A.; Zotti, L. A.; Lombardi, E. B.; Sabater, C.; Pakdel, S.; Palacios, J. J. A group-theoretic approach to the origin of chirality-induced spin selectivity in non-magnetic molecular junctions. 2022; arXiv:2211.04830.

(52) Michaeli, K.; Naaman, R. Origin of spin-dependent tunneling through chiral molecules. *The Journal of Physical Chemistry C* **2019**, *123*, 17043–17048.

(53) Wolf, Y.; Liu, Y.; Xiao, J.; Park, N.; Yan, B. Unusual Spin Polarization in the Chirality-Induced Spin Selectivity. *ACS Nano* **2022**, Article ASAP.

(54) Thoss, M.; Evers, F. Perspective: Theory of quantum transport in molecular junctions. *J. Chem. Phys.* **2018**, *148*, 030901.

(55) Cohen, G.; Galperin, M. Green's function methods for single molecule junctions. *J. Chem. Phys.* **2020**, *152*, 090901.

(56) Garner, M. H.; Li, H.; Chen, Y.; Su, T. A.; Shangguan, Z.; Paley, D. W.; Liu, T.; Ng, F.; Li, H.; Xiao, S.; Nuckolls, C.; Venkataraman, L.; Solomon, G. C. Comprehensive suppression of single-molecule conductance using destructive σ-interference. *Nature* **2018**, *558*, 415–419.

(57) Smidstrup, S.; Markussen, T.; Vancraeyveld, P.; Wellendorff, J.; Schneider, J.; Gunst, T.; Verstichel, B.; Stradi, D.; Khomyakov, P. A.; Vej-Hansen, U. G., et al. QuantumATK: An integrated platform of electronic and atomic-scale modelling tools. *J. Phys: Condens. Matter* **2020**, *32*, 015901.

(58) Ghiasi, T. S.; Kaverzin, A. A.; Blah, P. J.; van Wees, B. J. Charge-to-spin conversion by the Rashba–Edelstein effect in two-dimensional van der Waals heterostructures up to room temperature. *Nano letters* **2019**, *19*, 5959–5966.

(59) Wang, Z.; Ki, D.-K.; Chen, H.; Berger, H.; MacDonald, A. H.; Morpurgo, A. F. Strong interface-induced spin–orbit interaction in graphene on WS2. *Nature communications* **2015**, *6*, 1–7.

(60) Datta, S. *Electronic transport in mesoscopic systems*; Cambridge university press, 1997.

(61) Brandbyge, M.; Mozos, J.-L.; Ordejón, P.; Taylor, J.; Stokbro, K. Density-functional method for nonequilibrium electron transport. *Physical Review B* **2002**, *65*, 165401.

(62) Todorov, T. Spatial distribution of the electric current and field in atomic-scale conductors. *Philosophical Magazine B* **1999**, *79*, 1577–1590.

(63) Herrmann, C.; Reiher, M.; Hess, B. A. Comparative Analysis of Local Spin Definitions. *J. Chem. Phys.* **2005**, *122*, 034102.

(64) Cramer, C. J.; Truhlar, D. G. Density functional theory for transition metals and transition metal chemistry. *Phys. Chem. Chem. Phys.* **2009**, *11*, 10757–10816.

(65) Aragones, A. C.; Medina, E.; Ferrer-Huerta, M.; Gimeno, N.; Teixido, M.; Palma, J. L.; Tao, N.; Ugalde, J. M.; Giralt, E.; Diez-Perez, I.; Mujica, V. Measuring the Spin-Polarization Power of a Single Chiral Molecule. *small* **2017**, *13*, 1602519.

Graphical TOC Entry